

# Journal of Geophysical Research: Oceans

## RESEARCH ARTICLE

10.1002/2015JC011014

**Key Points:**

- Secular change in NPP off the shelf tracks changes in OWDs and SST
- Response of OWDs and NPP to SAM and ENSO was opposite for the shelf and off-shelf regions

**Correspondence to:**K. R. Arrigo,  
arrigo@stanford.edu**Citation:**

Schine, C. M. S., G. van Dijken, and K. R. Arrigo (2016), Spatial analysis of trends in primary production and relationship with large-scale climate variability in the Ross Sea, Antarctica (1997–2013), *J. Geophys. Res. Oceans*, 121, 368–386, doi:10.1002/2015JC011014.

Received 2 JUN 2015

Accepted 7 DEC 2015

Accepted article online 14 DEC 2015

Published online 11 JAN 2016

## Spatial analysis of trends in primary production and relationship with large-scale climate variability in the Ross Sea, Antarctica (1997–2013)

**Casey M. S. Schine<sup>1</sup>, Gert van Dijken<sup>1</sup>, and Kevin R. Arrigo<sup>1</sup>**<sup>1</sup>Department of Earth System Science, Stanford University, Stanford, California, USA

**Abstract** Recent studies have documented an increase in sea ice extent and the duration of the ice season in the Ross Sea, Antarctica. We conducted a satellite-based study to quantify changes in net primary production (NPP) and chlorophyll *a* (Chl *a*) in response to the observed changes in ice dynamics in the Ross Sea south of 60°S. Our study covers a 16 year time period (1997–2013) and incorporates both the shelf and off-shelf regions of the Ross Sea. We observed significant secular changes in NPP from 1997 to 2013 in the off-shelf region, with NPP increasing on the eastern side and decreasing on the western side of our study area. The changes we observed in NPP are consistent with the changes we observed in sea surface temperature (SST) and open water days (OWDs), decreasing (increasing) on the western (eastern) side of our study area. Finally, we examined the influence of the Southern Annular Mode (SAM) and the El Niño Southern Oscillation (ENSO), on SST, OWDs, Chl *a*, and NPP in the Ross Sea and observed a significant relationship between the state of the SAM and ENSO and SST, OWDs, and NPP across the study region. The response of OWDs, SST, and NPP to atmospheric forcing by SAM and ENSO was opposite for the shelf and off-shelf regions, such that during a positive phase of SAM or negative phase of ENSO (La Niña), SST, OWDs, and NPP increased on the shelf and decreased in the off-shelf region.

### 1. Introduction

The Ross Sea, located in the Pacific sector of the Southern Ocean to the southeast of New Zealand (Figure 1), harbors the most productive waters in the Antarctic [Arrigo *et al.*, 2008a]. Its off-shelf waters have an annual net primary production (NPP) rate of 428 Tg C a<sup>-1</sup> while its continental shelf (23.4 Tg C a<sup>-1</sup>) accounts for more than a third of Antarctic shelf NPP, despite comprising only 20% of Southern Ocean ice-free shelf area [Arrigo *et al.*, 2008a]. Primary production in the Ross Sea supports many upper trophic level organisms, including krill [Atkinson *et al.*, 2004], toothfish [Ainley *et al.*, 2012b], penguins [Ainley *et al.*, 2005], and whales [Ainley and Ballard, 2012], and is an important driver of oceanic CO<sub>2</sub> uptake [Arrigo *et al.*, 2008b]. On the Ross Sea shelf, iron input from the sediment [Arrigo *et al.*, 2015; Fitzwater *et al.*, 2000] and melting sea ice [Fitzwater *et al.*, 2000; Sedwick *et al.*, 2000] supports high rates of NPP (815 mg C m<sup>-2</sup> d<sup>-1</sup>) [Arrigo *et al.*, 2008a] during the austral spring and summer, resulting in low surface water pCO<sub>2</sub> (<200 μatm) [Tortell *et al.*, 2011]. Coupled with high carbon export efficiencies [Smith *et al.*, 2011], this low pCO<sub>2</sub> drives an influx of 20–50 g C m<sup>-2</sup> a<sup>-1</sup>, accounting for ~27% of the total Southern Ocean CO<sub>2</sub> sink [Arrigo *et al.*, 2008b].

Primary production in the Ross Sea shows a significant positive relationship with mean annual open water area both on and off the shelf [Arrigo and van Dijken, 2004, 2007; Arrigo *et al.*, 2008a]. A significant increase in sea ice has been reported for the Ross Sea since the beginning of the sea ice satellite record in 1979 [Comiso *et al.*, 2011; Liu *et al.*, 2004; Parkinson, 2002; Parkinson and Cavalieri, 2012; Simpkins *et al.*, 2012; Stammerjohn *et al.*, 2008, 2012; Turner *et al.*, 2009]. Comiso *et al.* [2011] reported an increase in ice cover in the Ross Sector, across all seasons, of 5% per decade, and Stammerjohn *et al.* [2008] found a 60 day decrease in the length of the open water season in the western Ross Sea since 1979.

The Southern Annular Mode (SAM) has been linked to interannual variability in sea ice extent (SIE) in the Ross Sea [Liu *et al.*, 2004; Sen Gupta and England, 2006; Stammerjohn *et al.*, 2008; Turner *et al.*, 2009] and it has been suggested that the increase in sea ice in the region since 1979 is the result of the summertime trend of the SAM toward its positive phase [Marshall, 2003; Marshall *et al.*, 2006; Stammerjohn *et al.*, 2008]. The SAM is the principal mode of atmospheric variability in the high-latitude Southern Hemisphere

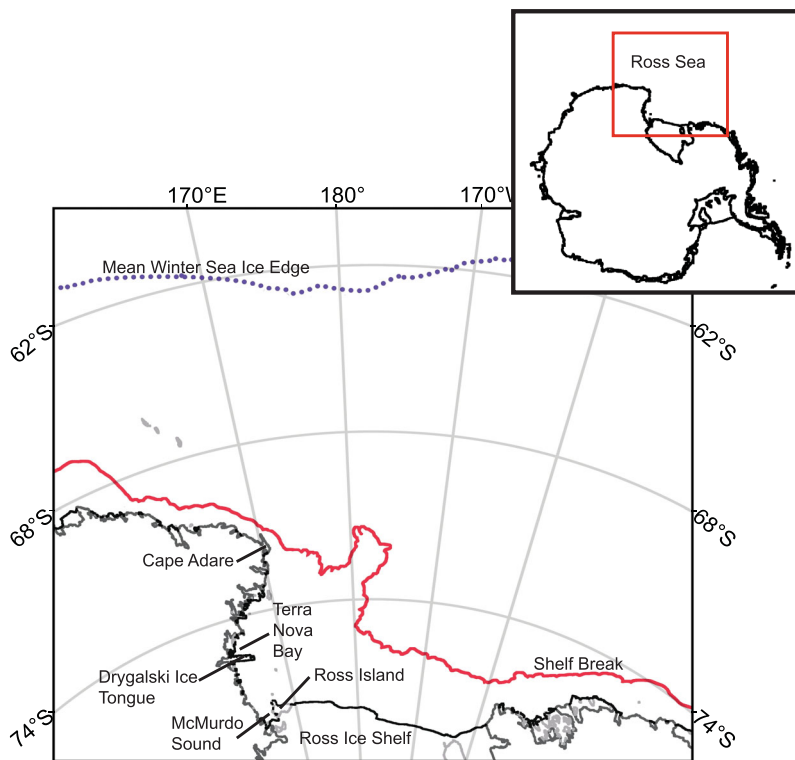


**Figure 1.** Map of the study area showing the location of the shelf break (the 1000 m isobath separating the on-shelf and off-shelf regions of the Ross Sea indicated by the solid red line) and the average location of the sea ice edge in winter (indicated by the dotted purple line). The mean winter sea ice edge was calculated from 1992 to 2013 using SSM/I brightness temperature with the PSSM algorithm as described in section 2.2. Coastline data are taken from the MODIS Mosaic of Antarctica (MOA) data set described in Scambos *et al.* [2007]. Bathymetry data were from SeaDAS version 6, which uses ETOPO2 water depths from the NOAA National Geophysical Data Center.

[Marshall, 2003; Thompson and Wallace, 2000], describing an annular gradient in sea level pressure (SLP) from higher pressures in the midlatitudes to low pressure over the Antarctic continent. This pressure gradient drives the westerly winds that circle Antarctica [Thompson and Wallace, 2000]. A positive phase of the SAM (+SAM) is characterized by positive SLP anomalies in the midlatitudes and negative SLP anomalies in the high latitudes, resulting in a stronger SLP gradient between the midlatitudes and high latitudes that drives an intensification and poleward shift of the westerly winds [Kwok and Comiso, 2002b; Lefebvre *et al.*, 2004]. The SAM is primarily zonal in structure, but the asymmetry of the Antarctic land mass results in an asymmetry in the SAM [Lachlan-Cope *et al.*, 2001] with a quasi-permanent low pressure center located to the west of the Antarctic Peninsula near the Amundsen and Bellingshausen Seas, called the Amundsen-Bellingshausen Seas Low (ABSL) [Fogt *et al.*, 2012]. Negative SLP anomalies in the ABSL during a positive phase of the SAM [Sen Gupta and England, 2006; Simpkins *et al.*, 2012] drive meridional winds [Lefebvre *et al.*, 2004]. During a positive SAM, the intensification of the westerly winds increases northward Ekman transport [Kwok and Comiso, 2002b; Liu *et al.*, 2004; Lovenduski and Gruber, 2005] and the meridional winds associated with the ABSL bring cold southerly winds into the Ross Sea [Lefebvre *et al.*, 2004; Liu *et al.*, 2004; Sen Gupta and England, 2006]. The combined effects of increased northward Ekman transport, wind-driven northward ice advection [Kwok and Comiso, 2002a; Turner *et al.*, 2015a, 2015b], and colder air temperatures are responsible for the positive sea ice anomalies observed in the Ross Sea region during a positive SAM [Liu *et al.*, 2004; Sen Gupta and England, 2006; Stammerjohn *et al.*, 2008; Turner *et al.*, 2009].

The El Niño Southern Oscillation (ENSO), generally thought of as a tropical phenomenon, has also been shown to have a significant influence on sea ice dynamics in the Ross Sea region [Kwok and Comiso, 2002a; Liu *et al.*, 2002; Stammerjohn *et al.*, 2008; Yuan, 2004]. The increase in sea ice in the Ross Sea region during La Niña (cold phase of ENSO) has been attributed to a spin-up of the ABSL [Fogt and Bromwich, 2006; Kwok

and Comiso, 2002a, 2000b; Yuan, 2004]. As with a positive phase of the SAM, negative SLP anomalies in the ABSL drive meridional winds, resulting in southerly winds over the Ross Sea [Kwok and Comiso, 2002a] that bring cold air from the continent into the region, resulting in decreased air temperature [Kwok and Comiso, 2002a; Liu et al., 2004] and northward ice advection [Kwok and Comiso, 2002a]. The ENSO polar teleconnection results from the stationary Rossby wave that propagates the tropical signal to the southern high latitudes [Karoly, 1989].

Our study will use the satellite records of sea ice, sea surface temperature (SST), and chlorophyll *a* (Chl *a*), as inputs to the NPP algorithm of Arrigo et al. [2008a], to examine how observed changes in sea ice have impacted NPP in the Ross Sea. We will investigate how NPP responds to atmospheric forcing by SAM and ENSO and examine how the finer resolution of our analysis impacts our interpretation of sea ice and SST dynamics in the region, relative to what has been reported previously.

## 2. Materials and Methods

### 2.1. Region of Interest

Our study region was confined to the area of the Ross Sea between 160°E and 155°W, south of 60°S (Figure 1). The northern boundary was set at 60°S as this is the approximate location of the polar front in this region [Kim and Orsi, 2014]. The polar front is characterized by a strong SST gradient, marking the boundary between warm subantarctic surface waters to the north and cold Antarctic surface waters to the south [Moore and Abbott, 2002]. The eastern and western boundaries were determined by the east/west boundaries of the Ross Sea. The shelf region was defined as the area with a depth less than or equal to 1000 m, and the off-shelf region as the area with a depth greater than 1000 m.

### 2.2. Satellite Data

Daily sea ice distribution (1992–2013) was computed from Special Sensor Microwave Imager (SSM/I) brightness temperatures obtained from the National Snow and Ice Data Center (University of Colorado, Boulder, CO), using the PSSM algorithm of Markus and Burns [1995], which produces high-resolution (6.25 km) maps of sea ice and open water area (rather than sea ice concentration) that are ideal for studying the smaller-scale sea ice dynamics on the Ross Sea shelf [Arrigo and van Dijken, 2004]. Our sea ice record only extends back to 1992 because in prior years, satellite sensors did not include the frequencies necessary for the PSSM algorithm.

Daily SST (1992–2013) was taken from Version 2 of the NOAA Daily Reynolds Optimally Interpolated SST [Reynolds et al., 2002]. Daily sea ice distribution was used to mask SST to ensure that data were only taken from areas of open water.

Chl *a* from level 2 SeaWiFS ocean color data (4 km resolution) processed using the OC4v4 algorithm [O'Reilly et al., 1998] were used for 1997–2002. The OC4v4 algorithm was chosen because it has been validated for the Ross Sea and shown to perform within 10% of in situ values [Arrigo and van Dijken, 2004]. Chl *a* from level 2 MODIS ocean color data (1 km resolution), processed using the OC3M algorithm [O'Reilly et al., 2000], were used for 2002–2013. The OC3M algorithm was developed using the same SeaBASS data set as the SeaWiFS OC4v4 algorithm and was chosen to be consistent with the OC4v4 algorithm used for the SeaWiFS data. Chl *a* data only extend back to 1997, the beginning of the SeaWiFS data record. We use the SeaWiFS and MODIS ocean color data as a seamless record, as the error between the Chl *a* estimates from the two satellites (with the OC4v4 and OC3M algorithms used here) is very small [Arrigo and van Dijken, 2011].

### 2.3. Net Primary Production

NPP at each pixel location was calculated hourly for 1997–2013, using the algorithm of Arrigo et al. [2008a], which has been extensively validated for the Southern Ocean. NPP was calculated using satellite-derived daily surface chlorophyll *a* (Chl *a*) concentrations, daily sea surface temperature (SST), monthly mixed layer depth (MLD), and hourly incident downwelling irradiance. Monthly MLD data were taken from the Naval Research Laboratory Mixed Layer Depth Climatologies [Kara et al., 2002], and hourly clear-sky downwelling irradiance was computed using the radiative transfer model of Gregg and Carder [1990]. To maximize spatial coverage, level 2 Chl *a* scenes were consolidated into daily composite images and daily composite images were averaged to create 5 day composite images. These 5 day composites were then used for daily Chl *a*

concentrations in the NPP algorithm for the 5 day period they represented. *Arrigo et al.* [2008a] present a detailed explanation of their Southern Ocean NPP algorithm and we therefore do not repeat that here.

#### 2.4. Climate Indices

The El Niño Southern Oscillation (ENSO) was characterized using the Multivariate ENSO Index (MEI) from the NOAA Earth System Research Laboratory [Wolter and Timlin, 1993, 1998]. We repeated our analyses involving the MEI with other ENSO indices (Niño 3, Niño 3.4, Southern Oscillation Index) and the results proved to be insensitive to the choice of index. The Southern Annular Mode (SAM) was characterized using the SAM index from *Marshall* [2003].

#### 2.5. Data Analysis

Annual values, used in subsequent calculations, were calculated for SST (1992–2013), Chl *a* (1997–2013), NPP (1997–2013), and open water days (OWDs; 1992–2013) from daily or multiday composite images. Annual mean SST was calculated for each pixel as the average of all SST values retrieved at that pixel in daily SST images from a given year. Annual mean Chl *a* concentration for each pixel was calculated as the average of all Chl *a* values retrieved at that pixel in 5 day composite Chl *a* images from a given year. Annual integrated NPP was calculated at each pixel location by multiplying the average daily NPP rate ( $\text{g C m}^{-2} \text{ d}^{-1}$ ) for that pixel for a given year by the number of open water days at that pixel for a given year, generating temporally integrated NPP ( $\text{g C m}^{-2} \text{ a}^{-1}$ ) for each year at each pixel location. Missing values were ignored in calculations of annual mean SST, annual mean Chl *a*, and annual integrated NPP. Annual OWDs were calculated as the number of open water days (OWDs) at each pixel location for a given year. The PSSM algorithm used here generates maps of open water and sea ice with a sharp gradient at the interface. We used a sea ice concentration cutoff of 50% for determining whether to count pixels at this interface as sea ice or open water. Because we are counting the number of open water days at each pixel, missing data values in our sea ice record would alter the annual count and therefore have to be filled in. Replacement values for missing data were calculated as an average of the values at that pixel for the day preceding and the day following the missing value. If a value at that pixel for either of those days was unavailable the next closest day (either preceding or following) was used. The difference in resolution between the SST images (0.25°) and the sea ice images (6.25 km) results in the striping observed in many of the images involving SST analyses. For one SST pixel, there are multiple sea ice pixels that each has a distinct number of OWDs. So for one SST pixel, the north side of the pixel may have a longer open water period than the south side. A longer open water period results in the inclusion of more winter values in the mean annual SST calculations, yielding a lower SST for the northern portion of the pixel than for the southern portion, resulting in the striping in our SST images. This striping is absent in our daily SST images.

Climatological means were calculated for SST (1992–2013; Figure 2a), OWDs (1992–2013; Figure 2d), Chl *a* (1997–2013; Figure 3a), and NPP (1997–2013; Figure 4a). For SST and Chl *a*, the climatological mean was calculated as the mean of all annual means for each pixel. For NPP, the climatological mean was calculated as the mean of annually integrated NPP for each year at each pixel. For OWDs, the climatological mean was calculated as the mean of the annual OWD counts at each pixel. The standard deviation on the climatological means was calculated for SST, OWDs, Chl *a*, and NPP (Figures 2b, 2e, 3b, and 4b, respectively).

We regressed SST, OWDs, Chl *a*, and NPP for each year at each pixel against time to look at secular changes, which we define as long-term temporal trends, for the study period (1992–2013 for SST and OWDs and 1997–2013 for Chl *a* and NPP). Chl *a* concentration and NPP were also regressed against SST and OWDs for each year, from 1997 to 2013, for each pixel to examine spatial relationships among the variables. SST, OWDs, Chl *a* concentration, and NPP for each year at each pixel were regressed against the mean SAM index and the mean MEI (both averaged from October through January) for each year in the study period (1992–2013 for SST and OWDs and 1997–2013 for Chl *a* and NPP) to look at the spatial response to atmospheric forcing by SAM and ENSO. We calculated linear regressions in IDL using the LINFIT() function, which fits the paired data to a linear model by minimizing the chi-square error statistic. We used the LINCORR() function in IDL to calculate *p*-values from the *t* statistic of the linear model and applying a two-sided *t* test to the result. Results were considered significant with a *p*-value  $\leq 0.05$ .

We examined trends in SST and OWDs over the entire length of our sea ice record, from 1992–2013 as opposed to 1997–2013 (the length of the ocean color record) as with the Chl *a* and NPP. We also examined

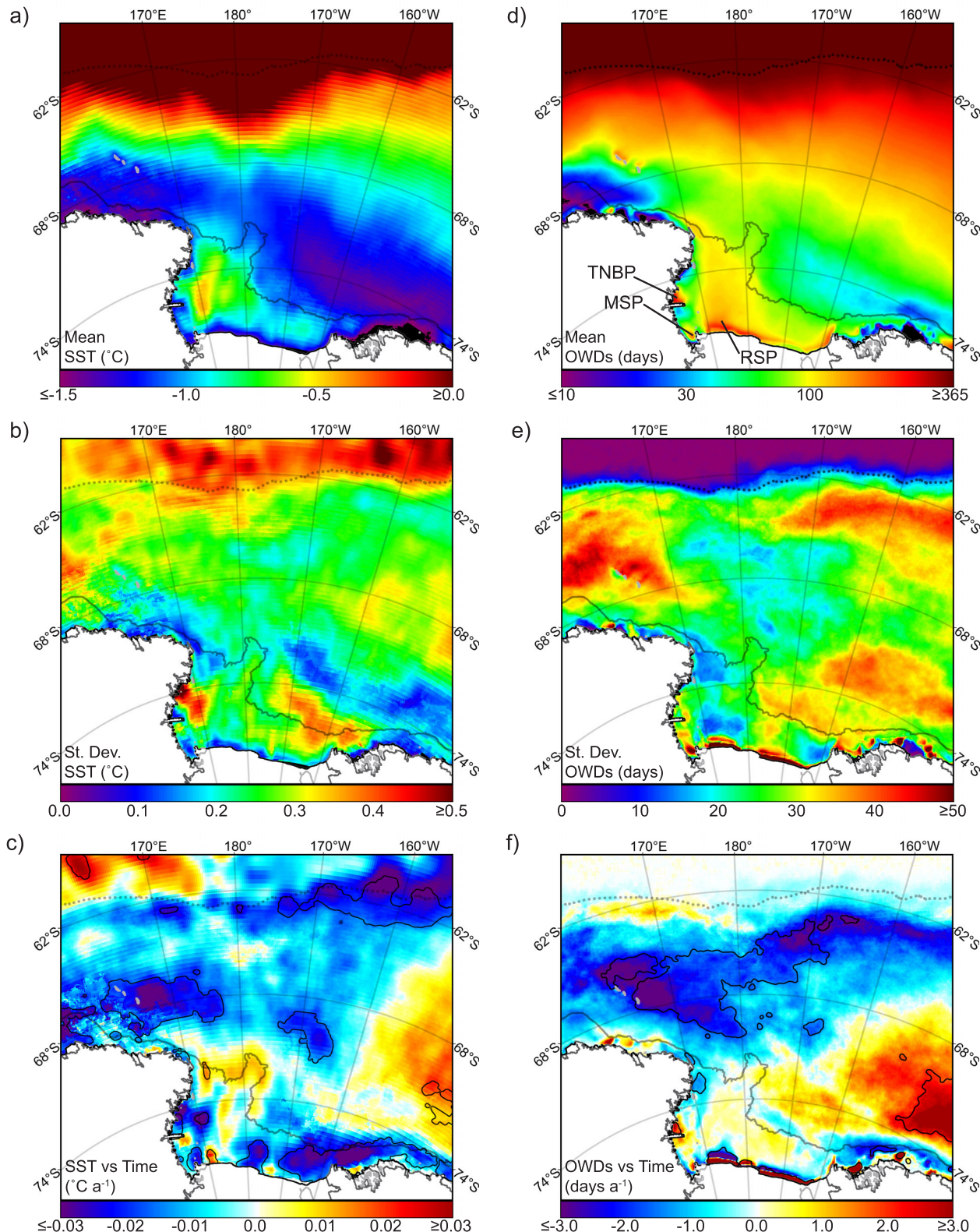


**Figure 2.** Maps of annual climatologies for (a) SST and (d) OWDs, the standard deviation associated with the annual climatologies for (b) SST and (e) OWDs, and (c) annual SST and (f) annual OWDs regressed against time. (d) Climatological mean OWDs are expressed on a logarithmic scale and the Ross Sea Polynya (RSP), Terra Nova Bay Polynya (TNBP), and McMurdo Sound Polynya (MSP) are labeled. Black outlines indicate a statistically significant relationship. The continental shelf break and the mean winter sea ice edge are shown as a solid gray line and a dotted gray line, respectively.

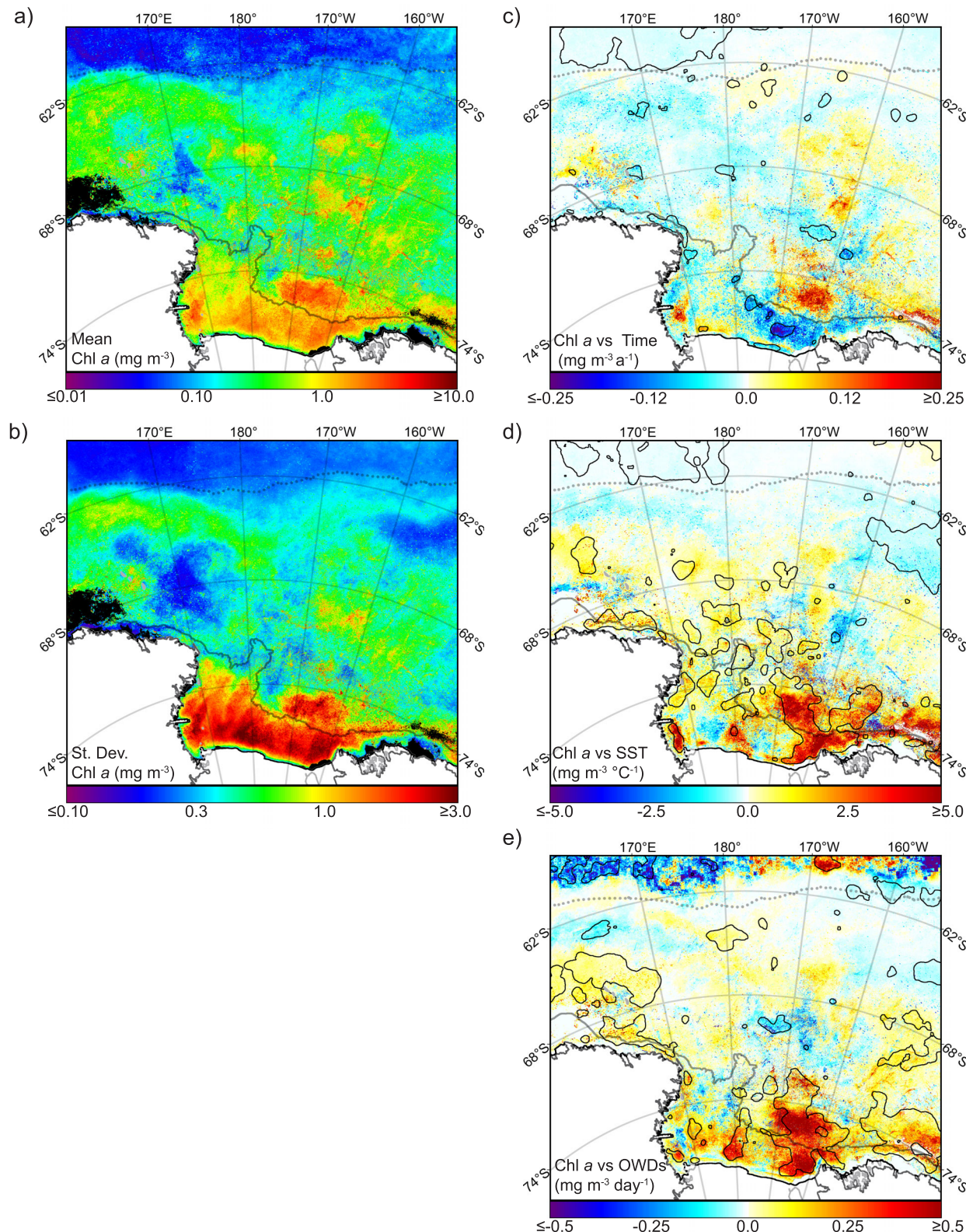


**Figure 3.** Maps of (a) annual climatology for Chl *a*, (b) the standard deviation associated with the annual climatology for Chl *a*, the slope of the regressions of (c) annual Chl *a* against time, (d) SST, and (e) OWDs. Climatological (a) mean and (b) standard deviation for Chl *a* are expressed on a logarithmic scale. Black outlines indicate a statistically significant relationship. The continental shelf break and the mean winter sea ice edge are shown as a solid gray line and a dotted gray line, respectively.

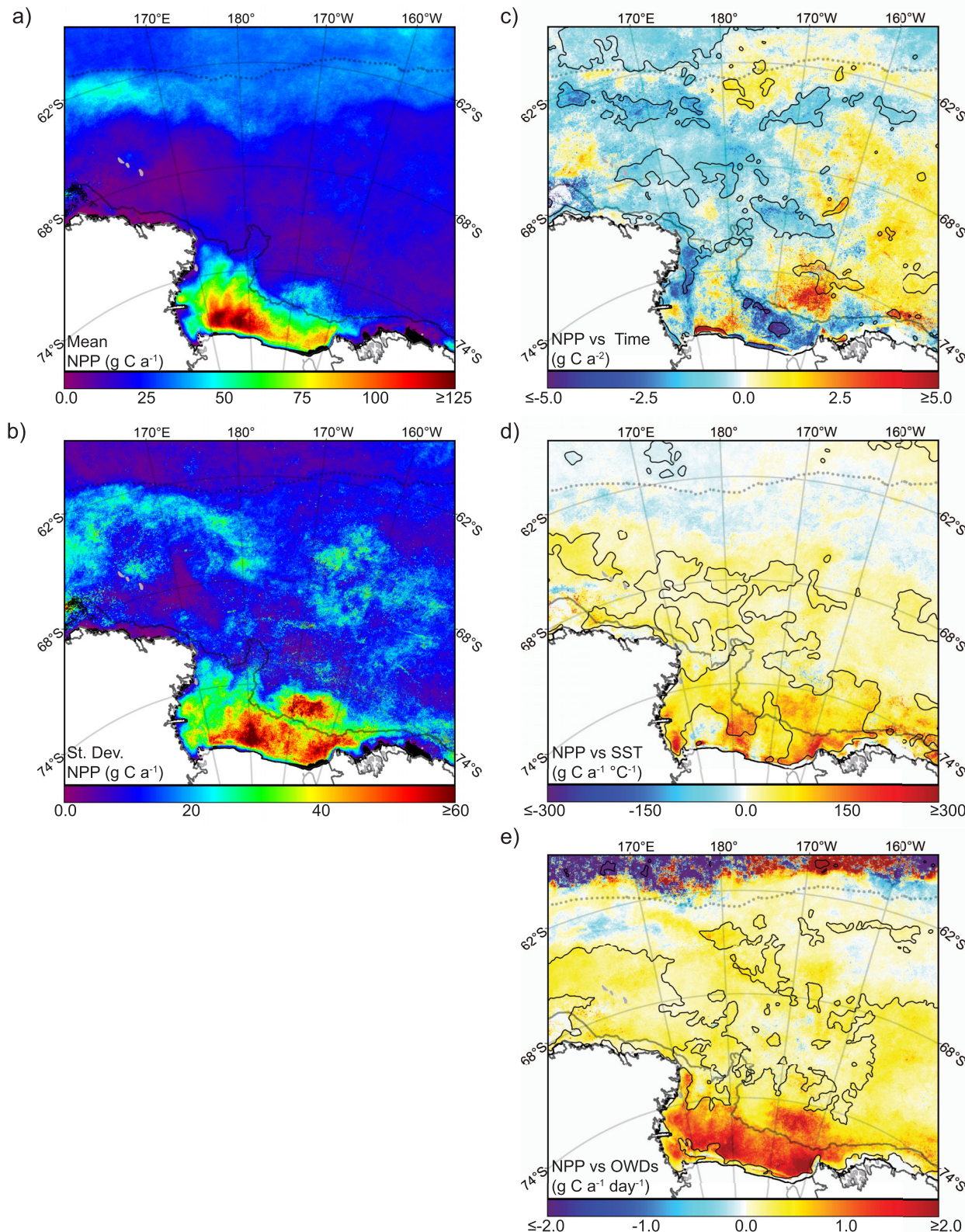


**Figure 4.** Maps of (a) annual climatology for NPP, (b) the standard deviation associated with the annual climatology for NPP, the slope of the regressions of (c) annual NPP against time, (d) SST, and (e) OWDs. Black outlines indicate a statistically significant relationship. The continental shelf break and the mean winter sea ice edge are shown as a solid gray line and a dotted gray line, respectively.

the impact of the longer time period on the trends observed in SST and OWDs both over time and in relation to the SAM and MEI and found that the inclusion of the additional 5 years of data increased the area of statistical significance but did not alter the direction or magnitude of the trends observed.

### 3. Results

#### 3.1. Sea Surface Temperature

On the Ross Sea continental shelf, waters were relatively warm ( $-1.0$  to  $-0.4^{\circ}\text{C}$ ), particularly to the north of Ross Island (Figure 2a). Immediately north of the shelf break was a band of much colder water ( $-1.2$  to  $-1.5^{\circ}\text{C}$ ), with increasingly warm SSTs farther to the north. This band of cold water north of the shelf break was also notable because it had the lowest amount of temporal variability in SST, with a standard deviation of  $0.1$ – $0.2^{\circ}\text{C}$  (Figure 2b). The area of highest variability in SST was in the north where the SST was highest, followed by two areas on the shelf, the first to the north of Terra Nova Bay, and the second on the eastern side of the shelf.

Between 1992 and 2013, SST increased significantly in some parts of the study region and decreased in others (Figure 2c). Spatially, the areas that showed a significant secular decrease in SST ( $-0.03$  to  $-0.02^{\circ}\text{C a}^{-1}$ ) were larger than areas that showed a significant increase in SST. The two areas on the shelf marked by higher SST variability (Figure 2b) overlapped with areas that exhibited a significant decrease in SST. In the northeastern corner of the study region (north of  $64^{\circ}\text{S}$  and west of  $175^{\circ}\text{W}$ ), the area with significantly decreased SST overlapped with a region of high SST variability (Figure 2b), and in the southeastern portion of the study region (north of the continental shelf and west of  $160^{\circ}\text{W}$ ), the area that showed a significant increase in SST also overlapped with an area of high SST variability.

#### 3.2. Sea Ice

The spatial pattern in mean annual OWDs on the shelf clearly showed the locations of the Ross Sea Polynya (RSP) north of the Ross Ice Shelf (RIS), the Terra Nova Bay Polynya (TNBP) north of the Drygalski Ice Tongue, and the McMurdo Sound Polynya (MSP) west of Ross Island (Figure 2d). These areas had a markedly longer period of open water ( $>100$  days) than the waters surrounding them. Sea ice was most persistent on the western side of the Ross Sea, west of Cape Adare (Figure 1), averaging  $<20$  OWDs per year.

In general, OWDs increased north of the shelf break up to the region of maximum winter SIE, beyond which the water was perennially ice free. OWDs along the northern sea ice edge were consistent between years, with a standard deviation of 10 days. OWDs had a standard deviation of 15–30 days throughout much of the study area (Figure 2e). However, throughout the sea ice zone, there were large patches of high interannual variability in OWDs, with a standard deviation as high as 50 days.

OWDs decreased significantly between 1992 and 2013 in a large swath across the off-shelf region of the study area, north of  $72^{\circ}\text{S}$  (Figure 2f). A significant increase in OWDs was apparent in the southeast portion of the study area north of the continental shelf (between  $68^{\circ}\text{S}$  and  $74^{\circ}\text{S}$ , east of  $160^{\circ}\text{W}$ ). The areas of significant secular change in OWDs per year (both increasing and decreasing) overlapped with the regions of high variability in OWDs (Figure 2e).

On the shelf, just north of the RIS, alternating stripes of significant increases and decreases in OWDs (Figure 2f) showed the effects of the large iceberg calving events that changed the face of the RIS since the year 2000 [Arrigo *et al.*, 2002; Robinson and Williams, 2012]. As the ice shelf edge has retreated in some places and advanced in others (in the center of the shelf), the location of the winter polynya has shifted to the south and north, respectively. This shift in the polynya has created very strong trends in OWDs immediately adjacent to the RIS. Terra Nova Bay has experienced a significant ( $2$ – $3 \text{ d a}^{-1}$ ) increase in OWDs between 1992 and 2013. On the shelf, north of Terra Nova Bay (north of  $74^{\circ}\text{S}$  on the  $170^{\circ}\text{E}$  meridian) are two small patches that showed a significant decrease in OWDs. These patches correspond with the northern projection of the RSP as it opens in the spring, suggesting that the land fast ice along the coast in this northern portion of the RSP has become more persistent.

#### 3.3. Chlorophyll *a*

Mean Chl *a* concentrations were highest on the shelf (Figure 3a), with a standard deviation from  $1.0$  to  $3.0 \text{ mg m}^{-3}$  over the majority of the region (Figure 3b). Between the continental shelf break and the

northern edge of the winter SIE, Chl *a* concentrations generally ranged from 0.1 to 0.8 mg m<sup>-3</sup>, with patches of higher Chl *a* scattered throughout the area. North of the edge of winter SIE, Chl *a* concentrations decreased to between 0.01 and 0.10 mg m<sup>-3</sup>. Variability in Chl *a* concentration between 1997 and 2013 (Figure 3b) closely mirrored the climatological mean Chl *a*, such that areas with high Chl *a* concentration corresponded to areas of high interannual variability and areas of low Chl *a* concentration corresponded to areas of low variability.

Only small patches of the Ross Sea exhibited a significant secular change in Chl *a* concentration between 1997 and 2013 (Figure 3c), with the exception of a large area in the northwest corner of the region (north of the edge of winter SIE and west of 180°) that experienced a significant decrease in mean annual Chl *a* concentration over the 15 year study period ( $-0.1 \text{ mg m}^{-3} \text{ a}^{-1}$ ). Several small patches in the southeastern portion of the shelf (east of 180°) experienced a significant decrease in mean annual Chl *a* concentration ( $-0.25 \text{ mg m}^{-3} \text{ a}^{-1}$ ).

Small patches where Chl *a* and SST showed a significant positive relationship are visible throughout the southern portion of the study region (south of 66°S; Figure 3d). A significant positive relationship between mean annual Chl *a* concentration and mean annual SST (up to 5 mg Chl *a* m<sup>-3</sup> °C<sup>-1</sup>) is apparent on the eastern side of the shelf, continuing north of the shelf break. This area is also a region of high SST variability (standard deviation of 0.4°C; Figure 2b). Two areas north of the shelf show a significant negative relationship between Chl *a* and SST (Figure 3d), one in the northwest (north of the edge of winter SIE and west of 180°) and the other on the eastern side of the study region (between 66°S and 62°S, east of 160°W). The area in the northwestern corner of the study region also showed a significant decrease in Chl *a* concentration between 1997 and 2013 (Figure 3c), as well as a significant increase in SST with time (Figure 2c), suggesting that SST is a factor in the declining Chl *a* concentrations seen in this area. The area to the east that shows a significant negative relationship between Chl *a* and SST (Figure 3d) did not show secular changes in either Chl *a* (Figure 3c) or SST (Figure 2c) but is an area of moderate SST variability (Figure 2b).

There was a significant positive relationship between Chl *a* concentration and number of OWDs on the shelf (up to 0.5 mg Chl *a* m<sup>-3</sup> d<sup>-1</sup>; Figure 3e). On the eastern side of the shelf, the positive relationship between Chl *a* and OWDs extends north of the shelf break. These areas also show a significant positive relationship between Chl *a* concentration and mean annual SST (Figure 3d).

### 3.4. Annual NPP

Annual NPP is highest on the shelf (up to 130 g C m<sup>-2</sup> a<sup>-1</sup>) and lowest (0 g C m<sup>-2</sup> a<sup>-1</sup> during some years) in a broad band to the north of the shelf break (Figure 4a) where the sea ice is most persistent (Figure 2d). Variability in mean annual NPP (Figure 4b) is highest (with areas  $\geq 60 \text{ g C m}^{-2} \text{ a}^{-1}$ ) on the shelf where annual NPP is highest. Variability in annual NPP is low north of the shelf break (0–10 g C m<sup>-2</sup> a<sup>-1</sup>) where mean annual NPP is lowest.

The strongest trend in NPP between 1997 and 2013 was found on the shelf (Figure 4c), with two areas, one to the east of the RSP (east of 180°) and one to the west (along the 170°E meridian), that experienced a significant decrease in NPP (up to 5 g C m<sup>-2</sup> a<sup>-1</sup>). The area to the east of the RSP saw a significant decrease in both SST (Figure 2c) and Chl *a* (Figure 3c). While, the area to the west of the RSP did not see a significant change in SST (Figure 2c), or Chl *a* (Figure 3c), a portion of it did experience a significant decrease in OWDs (Figure 2f). Two large areas in the off-shelf region of the Ross Sea also showed a significant trend in annual NPP between 1997 and 2013 (Figure 4c). Across the majority of the off-shelf region north of 72°S, with patches of significance concentrated on the western side, is a large area that experienced a moderate, but significant decrease in annual NPP over the study period ( $\sim 1 \text{ g C m}^{-2} \text{ a}^{-1}$  with patches as high as 3 g C m<sup>-2</sup> a<sup>-1</sup>). The majority of this area experienced a significant decrease in OWDs (Figure 2f) from 1992 to 2013, and parts of this area (north of the edge of winter SIE) also saw a significant decrease in Chl *a* concentration (Figure 3c). An area north of the shelf break in the southeast part of the study region (east of 170°W and south of 68°S) experienced a significant increase in annual NPP (up to 4 g C m<sup>-2</sup> a<sup>-1</sup>), corresponding with a significant increase in both OWDs (Figure 2f) and mean annual SST (Figure 2c).

There was a significant positive relationship between annual NPP and mean annual SST (Figure 4d) across the majority of the southern portion of the study region. The slope of this relationship was 100 g C m<sup>-2</sup> a<sup>-1</sup> °C<sup>-1</sup> across most of the study region and as high as 300 g C m<sup>-2</sup> a<sup>-1</sup> °C<sup>-1</sup> on the shelf. Areas with a

significant positive relationship between annual NPP and annual SST had a mean annual SST below  $-0.7^{\circ}\text{C}$  (Figure 2a), where even small changes in SST could have a large impact on NPP due to the nature of the relationship between phytoplankton growth and temperature [Arrigo *et al.*, 2008a]. A small area in the northwestern corner of the study region (north of the edge of winter SIE) showed a significant negative relationship between NPP and SST ( $-25 \text{ g C m}^{-2} \text{ a}^{-1} \text{ }^{\circ}\text{C}^{-1}$ ). This area also saw a significant decrease in NPP between 1997 and 2013 (Figure 4c) despite a significant increase in SST (Figure 2c) from 1992 to 2013. Annual NPP also showed a significant positive relationship with OWDs in the majority of the southern portion of the study region (Figure 4e). This relationship was strongest on the shelf (up to  $2 \text{ g C a}^{-1} \text{ d}^{-1}$ ) decreasing in the off-shelf region ( $0.3 \text{ g C a}^{-1} \text{ d}^{-1}$ ).

### 3.5. Climate Indices

On the shelf and extending north of the shelf break, the positive phase of the SAM was associated with significant increases in SST ( $0.10^{\circ}\text{C SAM}^{-1}$ ; Figure 5a), number of OWDs ( $15 \text{ d SAM}^{-1}$ ; Figure 5b), Chl *a* concentration ( $0.8 \text{ mg m}^{-3} \text{ SAM}^{-1}$ ; Figure 5c), and annual NPP ( $30 \text{ g C m}^{-2} \text{ a}^{-1} \text{ SAM}^{-1}$ ; Figure 5d). In off-shelf waters, a positive SAM was associated with a significant decrease in SST (up to  $-0.20^{\circ}\text{C SAM}^{-1}$ ) across the majority of the off-shelf area. The off-shelf response of OWDs to a positive SAM was split, showing a significant increase in OWDs to the west (as high as  $15 \text{ d SAM}^{-1}$ , north of  $68^{\circ}\text{S}$  and west of  $180^{\circ}$ ), and a significant decrease in OWDs to the east (as high as  $-15 \text{ d SAM}^{-1}$ , east of  $175^{\circ}\text{E}$  between  $64^{\circ}\text{S}$  and  $70^{\circ}\text{S}$ ). There was little apparent pattern of variation in Chl *a* with the SAM in the off-shelf region, except for a large portion of the eastern side of the study area (east of  $170^{\circ}\text{W}$  between  $64^{\circ}\text{S}$  and  $68^{\circ}\text{S}$ ) that exhibited a significant increase in Chl *a* concentration ( $0.3 \text{ mg m}^{-3} \text{ SAM}^{-1}$ ) despite significant decreases in SST and OWDs. Patches that showed a significant decrease in NPP in the off-shelf region ( $10 \text{ g C m}^{-2} \text{ a}^{-1} \text{ SAM}^{-1}$ ) during a positive phase of the SAM corresponded with decreased SST and decreased OWDs in the center of the study region (south of  $66^{\circ}\text{S}$  between  $170^{\circ}\text{E}$  and  $160^{\circ}\text{W}$ ). However, on the western side of the study region (north of  $65^{\circ}\text{S}$  and west of  $170^{\circ}\text{E}$ ), increased NPP corresponds with a significant increase in OWDs. Patches of increased NPP on the western margin of the off-shelf region (west of  $170^{\circ}\text{E}$  and south of  $65^{\circ}\text{S}$ ) corresponded with increased SST and increased OWDs. Additionally, the area on eastern side of the off-shelf region (east of  $165^{\circ}\text{W}$  between  $62^{\circ}\text{S}$  and  $68^{\circ}\text{S}$ ) that showed higher Chl *a* concentrations during a positive phase of the SAM did not show a significant increase in NPP.

During a positive phase of the MEI (El Niño), the shelf was characterized by a decrease in SST (with small patches of significance; Figure 6a), a decrease in OWDs (up to  $-20 \text{ d MEI}^{-1}$ ; Figure 6b), and a decrease in annual NPP (up to  $30 \text{ g C m}^{-2} \text{ a}^{-1} \text{ MEI}^{-1}$ ; Figure 6d). In contrast, the positive phase of the MEI was characterized in the off-shelf region by a significant increase in mean annual SST ( $0.1\text{--}0.2^{\circ}\text{C MEI}^{-1}$ ). While this pattern in SST is consistent in off-shelf waters, the pattern observed in OWDs is less uniform. A large area on the eastern side of the study region (extending from  $165^{\circ}\text{E}$  to the eastern edge of the study region) exhibited an increase in OWDs ( $10\text{--}20 \text{ d MEI}^{-1}$ ) and an increase in NPP ( $15 \text{ g C m}^{-2} \text{ a}^{-1} \text{ MEI}^{-1}$ ), while a smaller area to the west (west of  $175^{\circ}\text{E}$  just north of the shelf break) showed a significant decrease in OWDs (up to  $15 \text{ d MEI}^{-1}$ ). Chl *a* and NPP increased across the majority of the off-shelf region in response to a positive MEI.

## 4. Discussion

### 4.1. Secular Changes in SST, Sea Ice, and NPP

We observed significant secular changes in SST (Figure 2c) and the number of OWDs (Figure 2f) north of the continental shelf in the Ross Sea. The spatial pattern of secular change is similar for both SST and OWDs, with a large area spanning the off-shelf region having experienced a significant decrease, and an area on the eastern margin of the Ross Sea region, north of the shelf break, that experienced a significant increase. The significant decrease in OWDs observed across the off-shelf region in this study is consistent with the widely reported increase in SIE and the duration of the sea ice season [Comiso *et al.*, 2011; Liu *et al.*, 2004; Parkinson, 2002; Parkinson and Cavalieri, 2012; Simpkins *et al.*, 2012; Stammerjohn *et al.*, 2008, 2012] dating back to the beginning of the satellite sea ice record in 1979.

It is more difficult to find an appropriate comparison for the secular changes we observed in SST. Kwok and Comiso [2002b] reported a cooling of surface temperature in the western Ross Sea, and warming in the eastern Ross Sea, consistent with our findings. However, it is problematic to compare surface temperature in

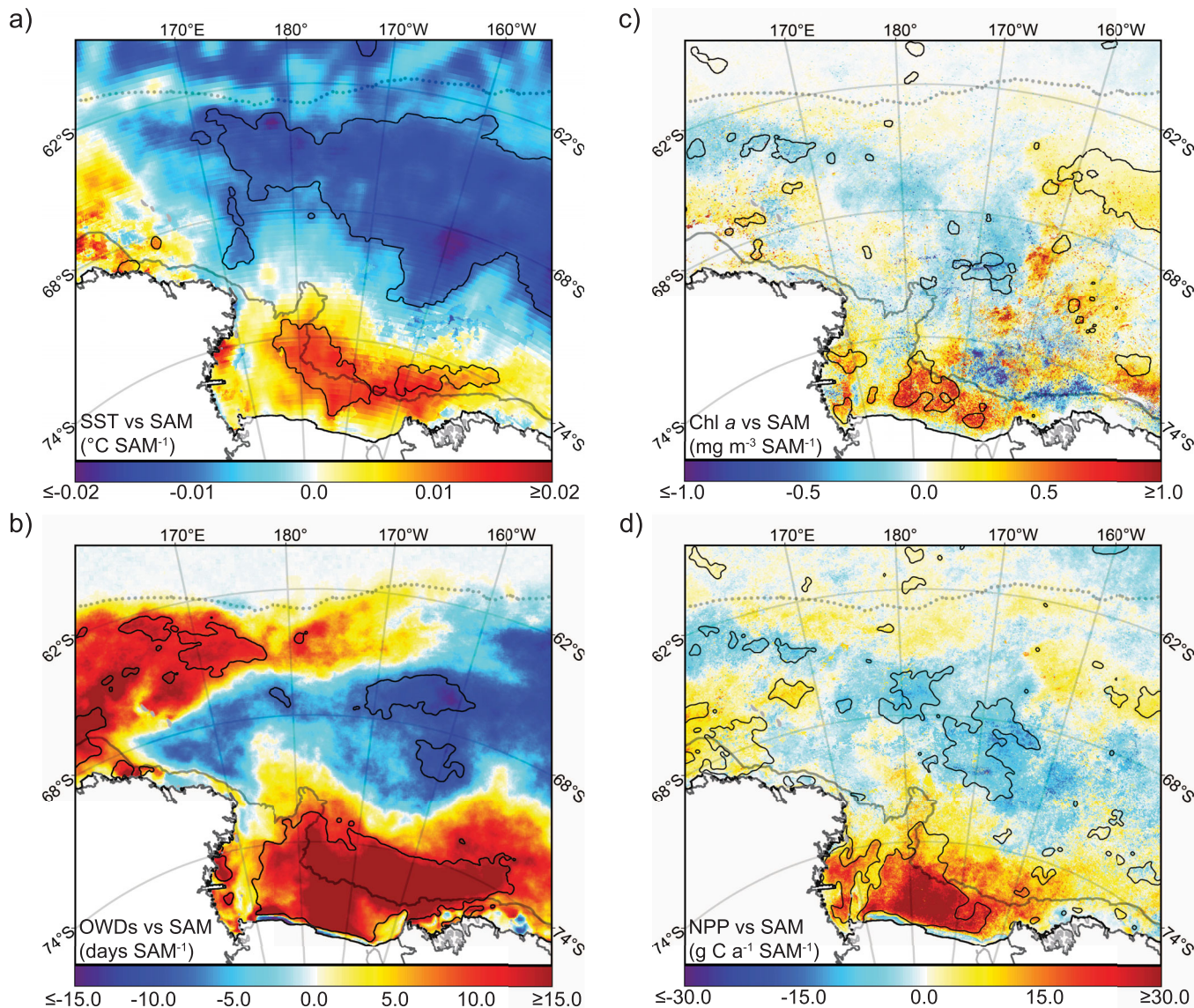


**Figure 5.** Maps of the slope of the regression of (a) SST, (b) OWDs, (c) Chl  $a$ , and (d) NPP against the SAM. Black outlines indicate a statistically significant relationship. The continental shelf break and the mean winter sea ice edge are shown as a solid gray line and a dotted gray line, respectively.

the Kwok and Comiso [2002b] study, which includes both ice surface temperature and sea surface temperature, with our SST measurements which only include surface temperature values from ice-free waters as determined by our daily ice images. Kwok and Comiso [2002b] explain that surface temperature data can be difficult to interpret because ice temperature will reflect water temperature when the ice is thin and air temperature when the ice is thicker. Liu et al. [2010] found a broad-scale warming trend in SST across the entire Southern Ocean, in contrast to the secular cooling observed in the Ross Sea in our study. The warming trend identified by Liu et al. [2010] occurred from 1950 to 1999, while our SST data extend from 1992 to 2013. With only 8 overlapping years, it is difficult to compare trends. The similarity in pattern between the secular changes in OWDs and SST indicates a link between the two variables. Arrigo et al. [2008a] reported a coincidence of positive SST anomalies and negative sea ice anomalies in the Ross Sea, consistent with the spatial overlap in our findings of decreased SST (Figure 2c) with decreased OWDs (Figure 2f) in the western portion of the off-shelf region, and increased SST with increased OWDs in the eastern portion of the off-shelf region. Arrigo et al. [2008a] concluded that the two variables were influencing each other, but stated, as is the case here, that causality is unclear.

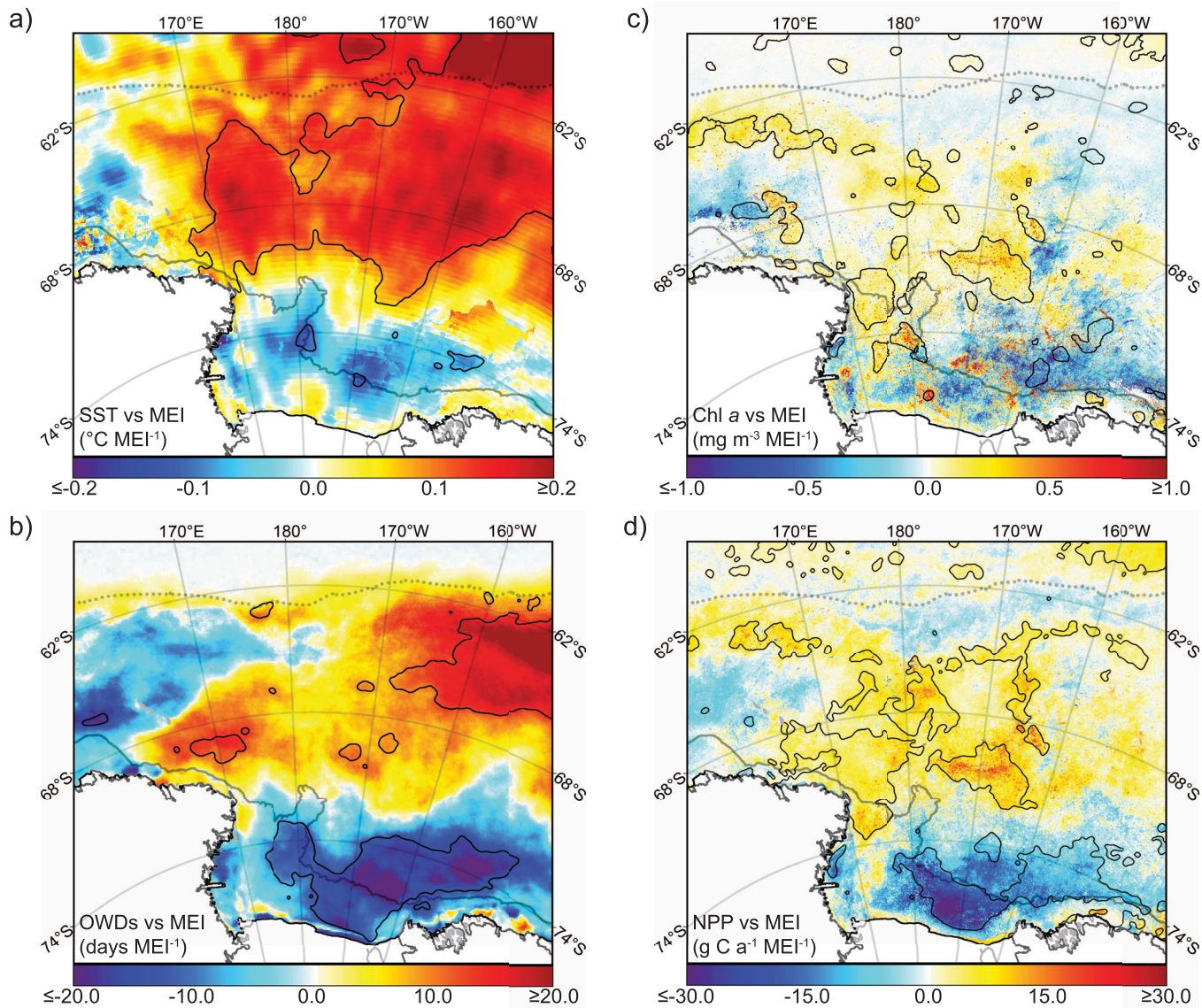


**Figure 6.** Maps of the slope of the regression of (a) SST, (b) OWDs, (c) Chl *a*, and (d) NPP against the MEI. Black outlines indicate a statistically significant relationship. The continental shelf break and the mean winter sea ice edge are shown as a solid gray line and a dotted gray line, respectively.

Significant secular changes in NPP are also apparent in the off-shelf region (Figure 4c), with a significant decrease in NPP on the western side of the region and a significant increase in NPP in the southeastern portion of our study region, a pattern similar to the secular changes in SST (Figure 2c) and OWDs (Figure 2f). The observed changes in NPP in the off-shelf region are most likely partially driven by the close relationship between NPP and both SST (Figure 4d) and OWDs (Figure 4e) in the southern portion of the Ross Sea. Our finding of a significant positive relationship between SST and NPP in the southern portion of the Ross Sea is consistent with the strong positive correlation between mean annual SST and mean annual NPP reported by Arrigo *et al.* [2008a] in the Ross Sea sector of the Southern Ocean. Arrigo *et al.* [2008a] further suggested that this relationship is the result of increased phytoplankton growth rates in warmer water. The secular changes in NPP are also driven by the significant positive relationship between NPP and OWDs (Figure 4e). Decreased NPP in the western portion of the study region is likely the result of a decrease in both SST and OWDs, while increased NPP on the eastern side of the off-shelf region is likely the result of increased SST and OWDs. This is consistent with the strong positive relationship between annual NPP and mean annual open water area reported by Arrigo *et al.* [2008a] in their pelagic province of the Ross Sea, which corresponds with the off-shelf region of our study area. This relationship is likely the result of increased light

availability driving an increase in phytoplankton growth rates. Our results expand on those of *Arrigo et al.* [2008a] by detailing the spatial relationships among NPP, SST, and OWDs for the Ross Sea.

Large areas on the shelf, relative to the entire shelf area, experienced a significant decrease in SST from 1992 to 2013, including a large contiguous area along the eastern side of the shelf (Figure 2c). This is consistent with the surface temperature cooling on the Ross Sea shelf from 1982 to 1999 shown by *Kwok and Comiso* [2002b]. This trend toward lower SST on the shelf may be driven by increased southerly winds [*Turner et al.*, 2015a, 2015b] and increased sea ice production [*Comiso et al.*, 2011] that have been reported for this region since 1979.

The shelf also showed small secular changes in OWDs along the RIS and in Terra Nova Bay (Figure 2c). The changes in OWDs seen along the edge of the RIS were due to the calving of several large icebergs in the years 2000 and 2002 that changed the shape of the RIS face [*Arrigo and van Dijken*, 2004], resulting in the winter polynya moving farther to the south. The increase in OWDs seen in the TNBP over the study period coincided with a decrease in SST. This is most likely due to an increase in the already frequent katabatic wind surges (daily average winds in excess of  $10 \text{ m s}^{-1}$ ) that have been reported in Terra Nova Bay [*Arrigo et al.*, 1998]. *Arrigo et al.* [1998] reported monthly climatological wind speeds adjacent to Terra Nova Bay that were twice as high as those coming off the RIS during the summer and 4 times higher during the winter. Our findings of only small regions of secular change in OWDs on the shelf are inconsistent with several studies that have shown significant increases in sea ice along the western side of the Ross Sea shelf [*Liu et al.*, 2004; *Simpkins et al.*, 2012; *Stammerjohn et al.*, 2008]. The inconsistency of our results with some of the previous reports of secular sea ice changes on the Ross Sea shelf may be the result of two things. First, we use a different, higher-resolution, ice product that has been specifically used to examine the small-scale sea ice dynamics on the Ross Sea shelf [*Arrigo and van Dijken*, 2004]. Second, our study period (1992–2013), which is constrained by the PSSM algorithm that we use to generate our sea ice images, is substantially different than the study period of other studies which begins in 1979, and in the case of [*Stammerjohn et al.*, 2008] only extends to 2004. In *Stammerjohn et al.* [2012], where they update their Southern Ocean sea ice duration calculations, the area on the Ross Sea shelf that has experienced a significant increase in sea ice persistence is notably smaller. It is possible that the inconsistency between our results and other reports of sea ice trends in the region is the combined effect of the scale of our sea ice images being more appropriate to the scale of sea ice dynamics on the Ross Sea shelf and the possibility we are reporting a more recent trend in sea ice that is only starting to become visible in the sea ice record that extends back to 1979.

NPP decreased significantly on the shelf in two patches, one to the east of the RSP and one to the west of the RSP (Figure 4c). The area to the east of the RSP also experienced a significant decrease in SST (Figure 2c) and Chl *a* (Figure 3c), but not OWDs (Figure 2d), while the area to the west of the RSP did not experience a significant change in any of these variables. NPP on the shelf showed a significant positive relationship with SST (Figure 4d), and it may be that the significant decrease in SST on the eastern side of the shelf is driving the significant decrease in NPP observed there. It is unclear what is driving the significant decrease in NPP on the western side of the shelf. NPP on the shelf showed a significant positive relationship with OWDs (Figure 4e), consistent with *Arrigo et al.* [2008a] who showed a strong relationship between annual NPP and mean annual open water area on the shelf. Despite the strong relationship between NPP and OWDs, the significant decreases in NPP observed on the shelf do not appear to be related to changes in OWDs as there were no significant secular trends in OWDs on the shelf.

#### 4.2. Similarity in Response of SST, Sea Ice, and NPP to Atmospheric Forcing by SAM and ENSO

The patterns we observed in SST, OWDs, and NPP due to the influence of SAM (Figure 5) are inverse to those of ENSO (Figure 6), such that the patterns for a +SAM closely resemble those for a −MEI (La Niña). Therefore, the patterns of coupled oceanic-atmospheric variability described by these indices possess similar impacts on the physical and biological environment of the Ross Sea. Starting in the 1990s, there has been an increase in the covariance of SAM and ENSO during the austral spring and summer, such that a positive SAM increasingly coincides with a La Niña (−MEI) [*Fogt and Bromwich*, 2006; *Simpkins et al.*, 2012]. As much as 25% of the variation in SAM is attributable to changes in ENSO during the austral summer [*L'Heureux and Thompson*, 2006]. The positive phase of the SAM is associated with an intensification of the surface westerlies, resulting in increased northward Ekman Transport [*Kwok and Comiso*, 2002b; *Liu et al.*, 2004; *Lovenduski and Gruber*, 2005], and an intensification of the ABSL, which drives meridional winds,

resulting in southerly winds across the Ross Sea [Lefebvre *et al.*, 2004] that bring colder air from the continent, causing a decrease in air temperature across the Ross Sea region [Lefebvre *et al.*, 2004; Liu *et al.*, 2004; Sen Gupta and England, 2006]. A La Niña phase of ENSO (negative MEI) is also associated with significant negative SLP anomalies in the ABSL [Fogt and Bromwich, 2006; Kwok and Comiso, 2002a, 2002b], which drives southerly winds over the Ross Sea [Kwok and Comiso, 2002a] that bring cold air from the continent into the study region, resulting in decreased air temperature [Kwok and Comiso, 2002a; Liu *et al.*, 2004] and northward ice movement [Kwok and Comiso, 2002a]. Both a +SAM and a -MEI generate northward ice movement and colder air temperatures in the Ross Sea.

#### 4.3. Opposing Response of Shelf and Off-Shelf Regions to Forcing by SAM and ENSO

The response of SST and sea ice to atmospheric forcing by SAM (Figures 5a and 5b) and ENSO (Figures 6a and 6b) on the continental shelf is opposite to that in the off-shelf region. During a positive phase of the SAM or a La Niña (-MEI), SST and OWDs increase both on the shelf and along the shelf break and decrease off the shelf. This stable and prominent feature in our analysis was also briefly described by Liu *et al.* [2004], and a close examination of the results of other previous studies of sea ice and SST in the Southern Ocean shows that the Ross Sea continental shelf behaves in opposition to the off-shelf region in response to atmospheric forcing by both SAM [Lefebvre *et al.*, 2004; Liu *et al.*, 2004; Simpkins *et al.*, 2012] and ENSO [Kwok and Comiso, 2002a; Liu *et al.*, 2004; Simpkins *et al.*, 2012; Stammerjohn *et al.*, 2008; Yuan, 2004]. While this phenomenon is apparent in other studies, this is the first time it has been explicitly identified as a major mode of variability in SST and OWDs in the Ross Sea in response to atmospheric forcing by SAM and ENSO. It is not surprising that the shelf region has been overlooked in larger scale studies, as the signal in the off-shelf region is the dominant feature in the regional response of sea ice and SST to atmospheric forcing by SAM and ENSO. The decrease in SST and sea ice (increased OWDs) that we observe during a +SAM/-MEI across the eastern portion of the off-shelf region is consistent with what has been previously reported for the Ross Sea [Arrigo and van Dijken, 2004; Kwok and Comiso, 2002a; Liu *et al.*, 2004; Lovenduski and Gruber, 2005; Sen Gupta and England, 2006; Simpkins *et al.*, 2012; Stammerjohn *et al.*, 2008; Yuan, 2004].

The response of Chl *a* and NPP to atmospheric forcing by SAM (Figures 5c and 5d) and ENSO (Figures 6c and 6d) follows a similar pattern to that of SST and OWDs, increasing on the shelf and decreasing off the shelf during a +SAM/-MEI. While no studies have looked at the response of Chl *a* or NPP to ENSO, Arrigo and van Dijken [2004] reported a significant increase in the mean annual Chl *a* concentration on the Ross Sea shelf during a +SAM, consistent with the increase in Chl *a* apparent on the shelf in our study. Arrigo *et al.* [2008a] also showed an increase in NPP on the shelf and a decrease off the shelf in response to a +SAM consistent with the results presented here, although neither of these trends was significant possibly due to the shorter time period of their study (1997–2006). In contrast, Lovenduski and Gruber [2005] showed an increase in Chl *a* concentration across the entire Ross Sea in response to a positive phase of the SAM, both on and off the shelf, inconsistent with the areas in the off-shelf region of our study that show a significant decrease in Chl *a* with a positive SAM. The remote sensing results presented by Lovenduski and Gruber [2005] cover a shorter time period (1997–2004) than the results from this study and Lovenduski and Gruber [2005] parse their data very differently from the data analysis methods presented here, which may explain the discrepancies between our findings. Lovenduski and Gruber [2005] looked at the correlation between Chl *a* concentrations and the state of the SAM in 8 day periods versus the annual periods examined in this study. The methods used by Lovenduski and Gruber [2005] highlight the short-term variations in both the SAM and Chl *a* concentrations while the methods used here look at how the state of the SAM impacts mean Chl *a* concentrations over the entire growing season, making it difficult to directly compare our results.

It has previously been proposed that the negative SST and positive sea ice anomalies reported in the Ross Sea region during a positive phase of the SAM are the combined result of increased northward Ekman transport due to the intensification of the westerly winds and decreased air temperature caused by the cold, southerly winds driven by the intensification of the ABSL [Liu *et al.*, 2004; Sen Gupta and England, 2006; Stammerjohn *et al.*, 2008; Turner *et al.*, 2009]. We hypothesize that the opposite response of SST and OWDs we observed on the shelf during a +SAM/-MEI is the result of southerly winds driven by the intensification of the ABSL advecting sea ice off the shelf and driving the upwelling of warm circumpolar deep water onto the shelf, resulting in increased SSTs and OWDs on the shelf, and decreased SST and OWDs off the shelf. Kwok and Comiso [2002a] observed an increase in southerly ice motion across the Ross Sea and a decrease

in westerly ice motion along the coast to the east of the Ross Sea during a La Niña phase of ENSO (−MEI); the opposite was true for an El Niño phase of ENSO (+MEI). Essentially, during a La Niña phase of ENSO, ice is being transported northward off the Ross Sea shelf, but then not continuing its journey to the east, resulting in an increase in OWDs on the shelf, and a decrease in OWDs off the shelf where the sea ice is accumulating. During El Niño, southerly winds decrease so ice is not advected to the north as quickly, but zonal winds along the coast have increased, so what little ice is present in the off-shelf region is being moved to the east. This results in a decrease in OWDs on the shelf, where the sea ice is lingering, and an increase in OWDs off the shelf, where the sea ice is being advected across the eastern boundary of our study region.

The response of OWDs to atmospheric forcing by SAM and ENSO is split in the off-shelf region of our study area, with OWDs in the east decreasing in response to +SAM/−MEI and OWDs in the west increasing. This divided response of OWDs in the off-shelf region of our study area is most likely due to the fact that the study region falls on the western edge of the area influenced by the ABSL [Stammerjohn *et al.*, 2008]. So the eastern side of the study region is experiencing the effects of the western edge of the meridional wind field created by the ABSL, while the western side of our study region is outside the influence of the ABSL. The edge of the influence of the ABSL is most pronounced in OWDs because of the movement of sea ice in this region, which is generally to the northeast [Holland and Kwok, 2012].

It has been suggested that the increase in sea ice that has been observed in the Ross Sea over the last 30 years is due to the strong positive SAM during the austral summer and autumn starting in the mid-1970s [Marshall, 2003; Marshall *et al.*, 2006; Stammerjohn *et al.*, 2008]. However, the spatial patterns that we see for SST, OWDs, Chl *a*, and NPP in response to atmospheric forcing by the SAM (Figure 5) do not match the patterns of secular change. First, the opposing responses in SST, OWDs, Chl *a*, and NPP of the shelf and off-shelf regions that we observe in response to atmospheric forcing by the SAM are absent in the patterns of secular change (Figures 2c, 2e, 3c, and 4c, respectively). Second, the area on the eastern margin of the study area that shows a secular increase in SST, OWDs, and NPP is absent in the response of these variables to the SAM. Finally, the area on the western margin of the study region that showed a significant increase in OWDs in response to a positive phase of the SAM is absent from the secular changes in OWDs observed in the region. The incongruence between the patterns of secular change in SST, OWDs, Chl *a*, and NPP and the response of these variables to the atmospheric forcing of the SAM is consistent with the findings of Simpkins *et al.* [2012] that trends in sea ice concentration from 1980 to 2008 were not related to SAM or ENSO, even during the austral summer when the trend toward a positive SAM is the strongest. Liu *et al.* [2004] found that the magnitude of the changes in sea ice associated with SAM and ENSO is much smaller than the regional sea ice trend in the Ross Sea from 1979 to 2002, and that the trends in SAM and ENSO could not explain the regional sea ice trends despite contributing significantly to the interannual variability in sea ice. Recently, it has been shown that the increase in sea ice extent and duration in the Ross Sea is partially a manifestation of an increase in the southerly winds over the Ross Sea resulting from an intensification of the ABSL since 1979 [Turner *et al.*, 2015a, 2015b]. As the deepening of the ABSL is only part of the atmospheric SLP response during a positive phase of the SAM, it could explain both the similarities we observe in the patterns of secular change in SST and sea ice and the patterns observed in response to atmospheric forcing by the SAM, as well as the differences.

#### 4.4. Broader Context

The spatial heterogeneity of the secular response of SST, OWDs, and NPP and the response of these variables to atmospheric forcing by SAM and ENSO apparent at the scale of our study provides an interesting context for understanding the impact of NPP variability on upper trophic levels and on the capacity of the Ross Sea region to act as a CO<sub>2</sub> sink. Phytoplankton are at the base of the foodweb in the Southern Ocean [Schofield *et al.*, 2010] and their rates of production may have a significant influence on both toothfish and penguin populations in the Ross Sea [Ainley *et al.*, 2012a, 2005]. A significant decline in the toothfish fishery in the Ross Sea has been documented since the beginning of commercial fishing in the region [Ainley *et al.*, 2012b] and it has been suggested that this may be due to a decrease in primary production on the Ross Sea shelf as a result of the increase in sea ice that has been reported for the region [Hanchet *et al.*, 2010]. Our results indicate that while there has been a significant decrease in NPP on the shelf in some areas, these decreases in NPP do not appear to be related to changes in OWDs and are not consistent across the shelf. Penguins, as sea ice obligates [Ainley *et al.*, 2005], are also impacted by changes in sea ice and NPP. Adélie penguins breed on land along the coast of the Ross Sea. They have been shown to benefit from summer

polynyas that are larger [Ainley *et al.*, 2005] and more productive [Arrigo and van Dijken, 2003], and colony size has been shown to be positively correlated with the SAM [Ainley *et al.*, 2005] due to the increase in OWDs on the shelf with a positive SAM. Adélie penguins overwinter in the off-shelf region of the Ross Sea on the pack ice close to the Antarctic Circle where they have enough light to forage [Ballard *et al.*, 2010; Wilson *et al.*, 2001]. Adélie penguin population growth is negatively correlated with maximum SIE [Wilson *et al.*, 2001] because penguins traveling from the Ross Sea breeding grounds to overwinter on the pack ice have a longer distance to travel and will use more energy for the journey than in years with less extensive sea ice [Ballard *et al.*, 2010]. Therefore, Adélie penguin populations may be impacted by changes in sea ice and production throughout a large portion of our study region. Ainley *et al.* [2005] also found that while Adélie penguin colony size on the Ross Sea shelf increased with increasing SAM, Emperor penguin colony size in Point Géologie decreased with increasing SAM. This finding is interesting in light of the divided response of sea ice to SAM across the Ross Sea region in this study. Point Géologie is on the coast of Adélie Land, adjacent to the portion of our study region that shows a decrease in OWDs in response to a positive SAM, which could explain why Emperor penguin colony size at Point Géologie shows a negative relationship with the SAM, while Adélie penguin colony size in the Ross Sea shows a positive relationship with the SAM. Both populations may increase in response to an increase in OWDs in the area, but experience a local increase in OWDs during opposite polarities of the SAM.

NPP by phytoplankton is also an important component of the biogeochemical cycle of carbon in the Ross Sea region due to the role of phytoplankton in carbon sequestration via the biological pump. It has been shown that the positive phase of the SAM is associated with CO<sub>2</sub> outgassing in the Ross Sea region of the Southern Ocean, resulting from the upwelling of DIC-rich water due to the intensification and poleward movement of the westerly winds [Hauck *et al.*, 2013; Lovenduski *et al.*, 2007] with a mean outgassing south of 55°S of 0.95 mol C m<sup>-2</sup> a<sup>-1</sup>. However, Arrigo and van Dijken [2007] showed that the Ross Sea shelf is a substantial CO<sub>2</sub> sink and maintains an influx of CO<sub>2</sub> on the shelf of 1.55 mol C m<sup>-2</sup> a<sup>-1</sup> during the low ice and high NPP conditions that our study has shown are characteristic of the positive phase of the SAM on the shelf.

## 5. Conclusion

The opposing response of the shelf and off-shelf regions to atmospheric forcing by SAM and ENSO, such that SST, OWDs, and NPP increase on the shelf and decrease off the shelf during a +SAM/-MEI, has not been previously identified as a significant mode of variability in the Ross Sea. We hypothesize that the mechanism responsible for the opposing response of the shelf region is the same as that previously described for the off-shelf region. The pressure in the ABSL decreases during a +SAM/-MEI, resulting in intensified southerly winds over the Ross Sea that bring cold air into the region, promoting sea ice persistence and northward movement that extends the sea ice edge further north during the winter. We hypothesize that these same southerly winds advect sea ice northward from the shelf into the off-shelf region where cold air temperatures and decreased zonal sea ice motion result in decreased sea ice on the shelf and increased in sea ice coverage off the shelf.

The secular changes that we observed in NPP in the off-shelf region from 1997 to 2013 closely tracked the changes observed in SST and OWDs, such that NPP increased where SST and OWDs increased and decreased where SST and OWDs decreased. It seems likely that this relationship will persist into the future. While the SAM cannot explain all the variability observed in sea ice and SST from 1992 to 2013, it does have a significant influence over sea ice and SST dynamics in the Ross Sea. The atmospheric pressure gradient from the midlatitudes to the high latitudes, described by the SAM, has been getting stronger during the summer since the 1970s (resulting in an increasingly positive SAM). Two mechanisms for the increased pressure gradient have been proposed; both rely on a temperature gradient between the midlatitudes and the high latitudes to drive the observed pressure gradient, but differ on the mechanism that generates the temperature gradient. The first proposed mechanism is stratospheric ozone depletion resulting in tropospheric cooling over the Antarctic continent [Lee and Feldstein, 2013; Thompson and Solomon, 2002; Thompson *et al.*, 2011], which increases the temperature gradient, and subsequently the pressure gradient, by cooling at the high latitudes. The second proposed mechanism is warming in the tropics due to the influence of rising greenhouse gas concentrations [Marshall *et al.*, 2004], which increases the temperature gradient and

the pressure gradient. If ozone depletion is driving the pressure gradient, we can expect to see a decrease in the pressure gradient with stratospheric ozone recovery, which should result in an increase in SST and OWDs and therefore, an increase in NPP, in the off-shelf region. However, if increasing greenhouse gas concentrations drive the pressure gradient, we should expect the tropical warming to persist and the pressure gradient to continue to increase, resulting in a decrease in SST and OWDs and a drop in NPP in the off-shelf region. If the two mechanisms are both at play, the pressure gradient between the midlatitudes and high latitudes will reflect the balance between warming over the Antarctic continent due to ozone recovery decreasing the pressure gradient and warming in the tropics increasing it. Predictions for the future of the SAM during the 21st century, from CMIP5 model simulations that include both greenhouse gas emissions and ozone recovery, favor a leveling off or a slight increase in the SAM. *Zheng et al.* [2013] showed that the balance between ozone recovery and greenhouse gas emissions will favor an increasingly positive SAM during the 21st century due to the influence of greenhouse gasses and tropical warming, while *Gillett and Fyfe* [2013] showed that the twentieth century positive trend in the SAM will level off in the 21st century as the effects of greenhouse gases and ozone recovery cancel each other out.

The future of the SAM also depends on the high-latitude teleconnection with ENSO. It has been shown that the ENSO/SAM teleconnection is reinforced when the two are in phase (+SAM/La Niña or −SAM/El Niño) such that a +SAM is more likely to occur during a La Niña [*Fogt and Bromwich*, 2006; *Fogt et al.*, 2011]. During out of phase occurrences (−SAM/La Niña or +SAM/El Niño), the magnitude of the high-latitude teleconnection is decreased [*Fogt et al.*, 2011]. *Cai et al.* [2014] project an increase in the occurrence of extreme El Niño events in the 21st century due to surface warming in the eastern equatorial pacific, which they predict will occur more rapidly than surrounding ocean waters. This increase in El Niño events has the potential to disrupt the teleconnection between ENSO and SAM which is predicted to be predominantly positive during the 21st century [*Gillett and Fyfe*, 2013; *Zheng et al.*, 2013]. In the absence of the influence of ENSO on the SAM, it is possible that we will see a different response in SST, sea ice, and NPP to the SAM in the future than the trends reported here. Covariance between ENSO and SAM has increased since the 1990s, with a +SAM increasingly coinciding with a La Niña [*Fogt and Bromwich*, 2006; *Simpkins et al.*, 2012]. Since the trends in SST, sea ice, and NPP in response to atmospheric forcing by SAM and ENSO that we report here only extend back to 1992, we are looking only at this period of strong covariance between SAM and ENSO. *Stammerjohn et al.* [2008] deconstructed the sea ice response to a + SAM with a La Niña and a +SAM without a La Niña during the 1990s. When a +SAM occurs with a La Niña the opposing response in sea ice between the shelf and off-shelf regions, that we identify here, is clearly apparent. However, the sea ice response to a +SAM without a La Niña shows a uniform increase in sea ice in the western Ross Sea extending from the shelf to the off-shelf region and decreasing sea ice in the off-shelf region of the eastern Ross Sea. It is possible that the predicted increase in the number of extreme El Niño events along with the predicted positive phase of the SAM during the 21st century will disrupt the SAM/ENSO teleconnection, resulting in a sea ice response to a +SAM similar to the one shown by *Stammerjohn et al.* [2008] for the 1990s, without the opposing response between the shelf and off-shelf regions reported here.

#### Acknowledgments

This work was supported by the National Science Foundation Office of Polar Programs (grant ANT1063592 to K.R.A.). We are also grateful for the input of K. E. Lowry and Z. W. Brown. Data to support this article are available upon request from the authors (casey@schine.net, arrigo@stanford.edu, gertvd@stanford.edu).

#### References

- Ainley, D. G., and G. Ballard (2012), Trophic interactions and population trends of killer whales (*Orcinus orca*) in the southern Ross Sea, *Aquat. Mammals*, 38(2), 153–160, doi:10.1578/AM.38.2.2012.153.
- Ainley, D. G., E. D. Clarke, K. R. Arrigo, W. R. Fraser, A. Kato, K. J. Barton, and P. R. Wilson (2005), Decadal-scale changes in the climate and biota of the Pacific sector of the Southern Ocean, 1950s to the 1990s, *Antarct. Sci.*, 17(2), 171–182, doi:10.1017/S0954102005002567.
- Ainley, D. G., C. M. Brooks, J. T. Eastman, and M. Massaro (2012a), Unnatural selection of Antarctic toothfish in the Ross Sea, Antarctica, in *Protection of the Three Poles*, edited by F. Huettmann, Springer, Japan, doi:10.1007/978-4-431-54006-9\_3.
- Ainley, D. G., N. Nur, J. T. Eastman, G. Ballard, C. L. Parkinson, C. W. Evans, and A. L. DeVries (2012b), Decadal trends in abundance, size and condition of Antarctic toothfish in McMurdo Sound Antarctica, 1972–2011, *Fish and Fisheries*, 14, 343–363, doi:10.1111/j.1467-2979.2012.00474.x.
- Arrigo, K. R., and G. L. van Dijken (2003), Phytoplankton dynamics within 37 Antarctic coastal polynya systems, *J. Geophys. Res.*, 108(C8), 3271, doi:10.1029/2002JC001739.
- Arrigo, K. R., and G. L. van Dijken (2004), Annual changes in sea-ice, chlorophyll *a*, and primary production in the Ross Sea, Antarctica, *Deep Sea Res., Part II*, 51, 117–138, doi:10.1016/j.dsrr.2003.04.003.
- Arrigo, K. R., and G. L. van Dijken (2007), Interannual variation in air-sea CO<sub>2</sub> flux in the Ross Sea, Antarctica: A model analysis, *J. Geophys. Res.*, 112, C03020, doi:10.1029/2006JC003492.
- Arrigo, K. R., and G. L. van Dijken (2011), Secular trends in Arctic Ocean net primary production, *J. Geophys. Res.*, 116, C09011, doi:10.1029/2011JC007151.
- Arrigo, K. R., A. M. Weiss, and W. O. Smith (1998), Physical forcing of phytoplankton dynamics in the southwestern Ross Sea, *J. Geophys. Res.*, 103(C1), 1007–1021.

- Arrigo, K. R., G. L. van Dijken, D. G. Ainley, M. A. Fahnestock, and T. Markus (2002), Ecological impact of a large Antarctic iceberg, *Geophys. Res. Lett.*, 29(7), doi:10.1029/2001GL014160.
- Arrigo, K. R., G. L. van Dijken, and S. Bushinsky (2008a), Primary production in the Southern Ocean, 1997–2006, *J. Geophys. Res.*, 113, C08004, doi:10.1029/2007JC004551.
- Arrigo, K. R., G. L. van Dijken, and M. Long (2008b), Coastal Southern Ocean: A strong anthropogenic CO<sub>2</sub> sink, *Geophys. Res. Lett.*, 35, L21602, doi:10.1029/2008GL035624.
- Arrigo, K. R., G. L. van Dijken, and A. L. Strong (2015), Environmental controls of marine productivity hot spots around Antarctica, *J. Geophys. Res. Oceans*, 120, 5545–5565, doi:10.1002/2015JC010888.
- Atkinson, A., V. Siegel, E. Pakhomov, and P. Rothery (2004), Long-term decline in krill stock and increase in salps within the Southern Ocean, *Nature*, 432, 100–103.
- Ballard, G., V. Toniolo, D. G. Ainley, C. L. Parkinson, K. R. Arrigo, and P. N. Trathan (2010), Responding to climate change: Adélie penguins confront astronomical and ocean boundaries, *Ecology*, 91(7), 2056–2069.
- Cai, W., et al. (2014), Increasing frequency of extreme El Niño events due to greenhouse warming, *Nat. Clim. Change*, 4, 111–116, doi:10.1038/nclimate2100.
- Comiso, J. C., R. Kwok, S. Martin, and A. L. Gordon (2011), Variability and trends in sea ice extent and ice production in the Ross Sea, *J. Geophys. Res.*, 116, C04021, doi:10.1029/2010JC006391.
- Fitzwater, S. E., K. S. Johnson, R. M. Gordon, K. H. Coale, and W. O. Smith (2000), Trace metal concentrations in the Ross Sea and their relationship with nutrients and phytoplankton growth, *Deep Sea Res., Part II*, 47, 3159–3179.
- Fogt, R. L., and D. H. Bromwich (2006), Decadal variability of the ENSO teleconnection to the high-latitude South Pacific governed by coupling with the Southern Annular Mode, *J. Clim.*, 19, 979–997.
- Fogt, R. L., D. H. Bromwich, and K. M. Hines (2011), Understanding the SAM influence on the South Pacific ENSO teleconnection, *Clim. Dyn.*, 36, 1555–1576.
- Fogt, R. L., A. J. Wovrosh, R. A. Langen, and I. Simmonds (2012), The characteristic variability and connection to the underlying synoptic activity of the Amundsen-Bellingshausen Seas Low, *J. Geophys. Res.*, 117, D07111, doi:10.1029/2011JD017337.
- Gillett, N. P., and J. C. Fyfe (2013), Annular mode changes in the CMIP5 simulations, *Geophys. Res. Lett.*, 40, 1189–1193, doi:10.1002/grl.50249.
- Gregg, W. W., and K. L. Carder (1990), A simple spectral solar irradiance model for cloudless maritime atmospheres, *Limnol. Oceanogr.*, 35(8), 1657–1675.
- Hanchet, S. M., S. Mornedre, and A. Dunn (2010), Bisttribution and relative abundance of Antarctic Toothfish (*Dissostichus mawsoni*) on the Ross Sea shelf, *CCAMLR Sci.*, 17, 33–51.
- Hauck, J., C. Volker, T. Wang, M. Hoppema, M. Losch, and D. A. Wolf-Gladrow (2013), Seasonally different carbon flux changes in the Southern Ocean in response to the Southern Annular Mode, *Global Biogeochem. Cycles*, 27, 1236–1245, doi:10.1002/2013GB004600.
- Holland, P. R., and R. Kwok (2012), Wind-driven tides in Antarctic sea-ice drift, *Nat. Geosci.*, 5, doi:10.1038/NGE01627.
- Kara, A. B., P. A. Rochford, and H. E. Hurlbert (2002), Naval Research Laboratory Mixed Layer Depth (NMLD) climatologies, report, 26 pp, Nav. Res. Lab., Washington, D. C.
- Karoly, D. J. (1989), Southern Hemisphere circulation features associated with El Niño-Southern Oscillation events, *J. Clim.*, 2, 1239–1252.
- Kim, Y. S., and A. H. Orsi (2014), On the variability of Antarctic circumpolar current fronts inferred from 1992–2011 Altimetry, *J. Phys. Oceanogr.*, 44, 3054–3071, doi:10.1175/JPO-D-13-0217.1.
- Kwok, R., and J. C. Comiso (2002a), Southern Ocean climate and sea ice anomalies associated with the Southern Oscillation, *J. Clim.*, 15, 487–501.
- Kwok, R., and J. C. Comiso (2002b), Spatial patterns of variability in Antarctic surface temperature: Connections to the Southern Hemisphere Annular Mode and the Southern Oscillation, *Geophys. Res. Lett.*, 29(14), doi:10.1029/2002GL015415.
- Lachlan-Cope, T. A., W. M. Connolley, and J. Turner (2001), The role of the non-axisymmetric Antarctic orography in forcing the observed pattern of variability of the Antarctic climate, *Geophys. Res. Lett.*, 28(21), 4111–4114.
- Lee, S., and S. B. Feldstein (2013), Detecting ozone- and greenhouse gas-driven wind trends with observational data, *Science*, 339, 563–567, doi:10.1126/science.1225154.
- Lefebvre, W., H. Goosse, R. Timmermann, and T. Fichefet (2004), Influence of the Southern Annular Mode on the sea ice-ocean system, *J. Geophys. Res.*, 109, C09005, doi:10.1029/2004JC002403.
- L'Heureux, M. L., and D. W. J. Thompson (2006), Observed relationships between the El Niño-Southern Oscillation and the Extratropical Zonal-Mean Circulation, *J. Clim.*, 19, 276–287.
- Liu, J., X. Yuan, D. Rind, and D. G. Martinson (2002), Mechanism study of the ENSO and southern high latitude climate teleconnections, *Geophys. Res. Lett.*, 29(14), doi:10.1029/2002GL015143.
- Liu, J., J. A. Curry, and D. G. Martinson (2004), Interpretation of recent Antarctic sea ice variability, *Geophys. Res. Lett.*, 31, L02205, doi:10.1029/2003GL018732.
- Liu, J., J. A. Curry, and M. H. Thiemanns (2010), Accelerated warming of the Southern Ocean and its impacts on the hydrological cycle and sea ice, *Proc. Natl. Acad. Sci. U. S. A.*, 107(34), 14,987–14,992, doi:10.1073/pnas.1003336107.
- Lovenduski, N. S., and N. Gruber (2005), Impact of the Southern Annular Mode on Southern Ocean circulation and biology, *Geophys. Res. Lett.*, 32, L11603, doi:10.1029/2005GL027277.
- Lovenduski, N. S., N. Gruber, S. C. Doney, and I. D. Lima (2007), Enhanced CO<sub>2</sub> outgassing in the Southern Ocean from a positive phase of the Southern Annular Mode, *Global Biogeochem. Cycles*, 21, GB2026, doi:10.1029/2006GB002900.
- Markus, T., and B. A. Burns (1995), A method to estimate subpixel-scale coastal polynyas with satellite passive microwave data, *J. Geophys. Res.*, 100(C3), 4473–4487.
- Marshall, G. J. (2003), Trends in the Southern Annular Mode from observations and reanalyses, *J. Clim.*, 16, 4134–4143.
- Marshall, G. J., P. A. Stott, J. Turner, W. M. Connolley, J. C. King, and T. A. Lachlan-Cope (2004), Causes of exceptional atmospheric circulation changes in the Southern Hemisphere, *Geophys. Res. Lett.*, 31, L14205, doi:10.1029/2004GL019952.
- Marshall, G. J., A. Orr, N. P. M. van Lipzig, and J. C. King (2006), The impact of a changing Southern Hemisphere annular mode on Antarctic Peninsula summer temperatures, *J. Clim.*, 19, 5388–5404.
- Moore, J. K., and M. R. Abbott (2002), Surface chlorophyll concentration in relation to the Antarctic Polar Front: Seasonal and spatial patterns from satellite observations, *J. Mar. Syst.*, 27, 69–86.
- O'Reilly, J. E., S. Maritorena, B. G. Mitchell, D. Siegel, K. L. Carder, S. Garver, M. Kahru, and C. McClain (1998), Ocean color chlorophyll algorithms for SeaWiFS, *J. Geophys. Res.*, 103(C11), 24,937–24,935.

- O'Reilly, J. E., et al. (2000), SeaWiFS post launch calibration and validation analyses, Part 3, report, 49 pp., NASA Goddard Space Flight Center, Greenbelt, Md.
- Parkinson, C. L. (2002), Trends in the length of the Southern Ocean sea-ice season, *Ann. Glaciol.*, **34**, 435–440.
- Parkinson, C. L., and D. J. Cavalieri (2012), Antarctic sea ice variability and trends, 1979–2010, *Cryosphere*, **6**, 871–880.
- Reynolds, R. W., N. A. Rayner, T. M. Smith, D. C. Stokes, and W. Wang (2002), An improved in situ and satellite SST analysis for climate, *J. Clim.*, **15**, 1609–1625.
- Robinson, N. J., and M. J. M. Williams (2012), Iceberg-induced changes to polynya operation and regional oceanography in the southern Ross Sea, Antarctica, from in situ observations, *Antarct. Sci.*, **24**(5), 514–526.
- Scambos, T. A., T. M. Haran, M. A. Fahnestock, T. H. Painter, and J. Bohlander (2007), MODIS-based Mosaic of Antarctica (MOA) data sets: Continent-wide surface morphology and snow grain size, *Remote Sens. Environ.*, **111**, 242–257, doi:10.1016/j.rse.2006.12.020.
- Schofield, O., H. W. Ducklow, D. G. Martinson, M. P. Meredith, M. A. Moline, and W. R. Fraser (2010), How do polar marine ecosystems respond to rapid climate change?, *Science*, **328**, 1520–1523.
- Sedwick, P. N., G. R. DiTullio, and D. J. Mackey (2000), Iron and manganese in the Ross Sea, Antarctica: Seasonal iron limitation in Antarctic shelf waters, *J. Geophys. Res.*, **105**(C5), 11,321–11,336, doi:10.1029/2000JC000256.
- Sen Gupta, A., and M. H. England (2006), Coupled ocean-atmosphere-ice response to variations in the Southern Annular Mode, *J. Clim.*, **19**, 4457–4486.
- Simpkins, G. R., L. M. Ciasto, D. W. J. Thompson, and M. H. England (2012), Seasonal relationships between large-scale climate variability and Antarctic sea ice concentration, *J. Clim.*, **25**, 5451–5469, doi:10.1175/JCLI-D-11-00367.1.
- Smith, W. O. J., A. R. Shields, J. C. Dreyer, J. A. Peloquin, and V. L. Asper (2011), Interannual variability in vertical export in the Ross Sea: Magnitude, composition, and environmental correlates, *Deep Sea Res. Part I*, **58**, 147–159, doi:10.1016/j.dsr.2010.11.007.
- Stammerjohn, S. E., D. G. Martinson, R. C. Smith, X. Yuan, and D. Rind (2008), Trends in Antarctic annual sea ice retreat and advance and their relation to El Niño-Southern Annular Mode variability, *J. Geophys. Res.*, **113**, C03S90, doi:10.1029/2007JC004269.
- Stammerjohn, S. E., R. Massom, D. Rind, and D. Martinson (2012), Regions of rapid sea ice change: And inter-hemispheric seasonal comparison, *Geophys. Res. Lett.*, **39**, L06501, doi:10.1029/2012GL050874.
- Thompson, D. W. J., and S. Solomon (2002), Interpretation of recent Southern Hemisphere climate change, *Science*, **296**, 895–899, doi:10.1126/science.1069270.
- Thompson, D. W. J., and J. M. Wallace (2000), Annular modes in the extratropical circulation. Part I: Month-to-month variability, *J. Clim.*, **13**, 1000–1016.
- Thompson, D. W. J., S. Solomon, P. J. Kushner, M. H. England, K. M. Grise, and D. J. Karoly (2011), Signatures of the Antarctic ozone hole in Southern Hemisphere surface climate change, *Nat. Geosci.*, **4**, 741–749, doi:10.1038/ngeo1296.
- Tortell, P. D., C. Gueguen, M. C. Long, C. D. Payne, P. Lee, and G. R. DiTullio (2011), Spatial variability and temporal dynamics of surface water  $\text{pCO}_2$ ,  $\text{O}_2/\text{Ar}$  and dimethylsulfide in the Ross Sea, Antarctica, *Deep Sea Res., Part I*, **58**, 241–259, doi:10.1016/j.dsr.2010.12.006.
- Turner, J., J. C. Comiso, G. J. Marshall, T. A. Lachlan-Cope, T. Bracegirdle, T. Maksym, M. P. Meredith, Z. Wang, and A. Orr (2009), Non-annular atmospheric circulation change induced by stratospheric ozone depletion and its role in the recent increase of Antarctic sea ice extent, *Geophys. Res. Lett.*, **36**, L08502, doi:10.1029/2009GL037524.
- Turner, J., J. S. Hosking, T. J. Bracegirdle, G. J. Marshall, and T. Phillips (2015a), Recent changes in Antarctic sea ice, *Philos. Trans. R. Soc. A*, **373**, 20140163, doi:10.1098/rsta.2014.0163.
- Turner, J., J. S. Hosking, G. J. Marshall, T. Phillips, and T. J. Bracegirdle (2015b), Antarctic sea ice increase consistent with intrinsic variability of the Amundsen Sea Low, *Clim. Dyn.*, **1**–12, doi:10.1007/s00382-015-2708-9.
- Wilson, P. R., D. G. Ainley, N. Nur, S. S. Jacobs, K. J. Barton, G. Ballard, and J. C. Comiso (2001), Adélie penguin population change in the Pacific sector of Antarctica: Relation to sea-ice extent and the Antarctic Circumpolar Current, *Mar. Ecol. Prog. Ser.*, **213**, 301–309.
- Wolter, K., and M. S. Timlin (1993), Monitoring ENSO in COADS with a seasonally adjusted principal component index, paper presented at the 17th Climate Diagnostics Workshop, NOAA/NMC/CAC, NSSL, Okla. Clim. Surv., CIMMS and the School of Meteorol., Univ. of Okla., Norman.
- Wolter, K., and M. S. Timlin (1998), Measuring the strength of ENSO events: How does 1997/98 rank?, *Weather*, **53**, 315–324.
- Yuan, X. (2004), ENSO-related impacts on Antarctic sea ice: A synthesis of phenomenon and mechanisms, *Antarct. Sci.*, **16**(4), 415–425, doi:10.1017/S0954102004002238.
- Zheng, F., J. Li, R. T. Clark, and H. C. Nnamchi (2013), Simulation and projection of the Southern Hemisphere Annular Mode in CMIP5 models, *J. Clim.*, **26**, 9860–9879, doi:10.1175/JCLI-D-13-00204.1.